Speed sensorless control performance improvement of induction motor drive using uncertainty cancellation

K.H.Chao and C.M.Liaw

Abstract: An improved speed estimator using parameter uncertainty cancellation and its application to an indirect field-oriented induction motor drive are presented. First, the speed estimation errors of a V-I model-based adaptive speed observer due to parameter variations are analysed. Then, accordingly, a novel compensation scheme is developed to cancel the effects of parameter variations on the estimated speed performance. A variable structure system controller, with the detected error signal as its input, is employed to realise the proposed compensation scheme. Finally, the robust speed control with quantitative control performance considering the effect of dead-time enlargement due to the feedback of estimated speed is presented. Theoretic bases of the proposed speed estimator and the robust speed controller are derived in detail, and their validities are demonstrated by some simulation and measured results.

1 Introduction

In recent decades, many speed estimation and sensorless control approaches for induction motor drives have been proposed and surveyed in [1]. These approaches can be roughly categorised into the rotor slot ripple method, high-frequency current injection method, extended Kalman filter technique and the application of model reference adaptive control. The common limitation of the latter three groups of approaches is that the resulting motor drive performances are not robust, as some of the motor parameters are employed.

One of the sensorless control approaches most frequently applied, in conjunction with indirect field-oriented (IFO) control of the induction motor drive, is perhaps the model reference adaptive control (MRAC) [2, 3]. In this method, two error functions, generated from flux estimation schemes based on voltage and current models, are used for adaptively tuning the rotor speed. Hyperstability is employed to handle the stability of the whole adaptive estimation mechanism. This method will be referred to as the V-I model-based speed observer hereafter in this paper. However, unfortunately, this method also uses the motor parameters, such as stator resistance, stator inductance and rotor time constant, that vary highly during operation. The variations are mainly due to temperature rise, magnetic saturation and skin effect.

Some studies on the effects of parameter variations on the speed estimation and sensorless control performances of the V-I model estimation approach have been made in [4–10]. In [4], only the effect of rotor resistance change on the speed estimation and field-orientation characteristics was studied. The impact and evaluation of all key parameter variations on speed estimation in a sensorless field-oriented induction motor drive have been studied in [5, 10]. Some valuable phenomena are revealed via simulation results. However, no transfer functions representing error dynamics and measured results are provided. In the small signal stability analysis made by Gimenez *et al.* [6], it has been found that incorrect parameters can give rise to the speed estimates corrupted by transient oscillations.

Comparative studies of the effects of speed estimator parameter variations on model reference adaptive systems and extended Kalman filter approaches have been performed in [7], wherein there is still no error dynamic model derived. The study made in [8] emphasised the accuracy and robustness limitations of the sensorless control, but no analytical results of error dynamic behaviour are provided. As for [9], only the static speed error caused by stator resistance variation is studied.

Many studies related to the improvement of this control approach have been made in [11–15]. A secondary resistance identification method proposed in [11] can let the secondary resistance converge to its correct value, but the convergence speed is low [15], so that a good dynamic response is rather difficult to obtain. In addition, the estimated speed is still sensitive to the variations in stator resistance, leakage inductances and magnetising inductance.

An improved motor speed identification scheme for an IFO induction motor drive has been proposed in [12]. In this scheme, a mutual MRAC containing two interchangeable models is proposed to implement the sensorless control of the motor. Pure integration and stator leakage inductance are not employed in the reference model, and the stator resistance is on-line identified. However, the estimated stator resistance is accurate only when the rotor speed is constant over a brief interval, and the estimated speed performance is still affected by the rotor inductance and magnetising inductance changes. Dynamic performance improvement via on-line tuning for the rotor time constant and stator resistance has also been achieved in [13]. In addition to these, research is still being carried out [14, 15] into improving the sensorless control performance of induction motors by estimating some motor parameters,

IEE Proceedings online no. 20000405

DOI: 10.1049/ip-epa:20000405

Paper first received 19th October 1999 and in revised form 23rd February 2000

The authors are with the Department of Electrical Engineering, National Tsing Hua University, Hsinchu, Taiwan, Republic of China

but the parameter insensitive control performance is still difficult to achieve.

In this paper, an induction motor speed estimator that uses a parameter uncertainty cancellation technique by means of variable structure system (VSS) control is developed. First, the speed estimation errors of the so-called V-I model-based estimator caused by the key motor parameter variations are analysed in detail. The transfer function models representing these error dynamics are derived. Then, a VSS compensation controller is developed to reduce the parameter uncertainty effects on the speed sensorless control performance.

In addition to the improvement in speed estimation, the speed control dynamic response improvement of the speed sensorless IFO induction motor drive is also studied in this paper. First, a dynamic model representing the dynamic behaviour of the IFO induction motor drive under the proposed speed sensorless control is established. Based on the estimated linear model [16] at the chosen nominal operating condition, a proportional plus integral-derivative (PI-D) two-degree-of-freedom (2DOF) speed controller [17] is systematically designed to fulfil the prescribed control specifications. Then, to reduce the speed control performance degradation due to the system parameter variations and the effect of dead-time, a robust controller (RC) [18, 19] with a dead-time compensator [19] is designed. Some simulation and measured results are provided to show the performance of the motor drive using the proposed sensorless control approach.

2 V-I model-based MRAC speed estimator

The state equations of a squirrel-cage induction motor in the stationary reference frame can be expressed as follows [20]:

$$\begin{bmatrix} v_{qs} \\ v_{ds} \\ 0 \\ 0 \end{bmatrix} = \begin{bmatrix} R_s + p\delta & 0 & \frac{pL_m}{L_r} & 0 \\ 0 & R_s + p\delta & 0 & \frac{pL_m}{L_r} \\ \frac{-L_m R_r}{L_r} & 0 & \frac{R_r}{L_r} + p & -\omega_r \\ 0 & \frac{-L_m R_r}{L_r} & \omega_r & \frac{R_r}{L_r} + p \end{bmatrix} \times \begin{bmatrix} i_{qs} \\ i_{ds} \\ \lambda_{qr} \\ \lambda_{dr} \end{bmatrix} \tag{1}$$

$$T_e = \frac{3}{4} P \frac{L_m}{L_r} (i_{qs}\lambda_{dr} - i_{ds}\lambda_{qr}) = T_L + B\omega_r + Jp\omega_r \tag{2}$$

where $p \triangleq d/dt$; $\delta \triangleq L_s - L_m^2/L_r$; J = total mechanical inertia; B = total damping coefficient; and the meanings of the other variables and parameters are clear from the literature [20]. From eqn. 1, the following voltage model and current model rotor flux equations can be derived [2]:

voltage model:

$$\begin{aligned} p\lambda_{qrv} &= (L_r/L_m)(v_{qs} - R_s i_{qs} - \delta p i_{qs}) \\ p\lambda_{drv} &= (L_r/L_m)(v_{ds} - R_s i_{ds} - \delta p i_{ds}) \end{aligned} \tag{3}$$

current model:

$$\begin{aligned} p\lambda_{qri} &= -(R_r/L_r)\lambda_{qri} + \omega_r \lambda_{dri} + (L_m R_r/L_r) i_{qs} \\ p\lambda_{dri} &= -(R_r/L_r)\lambda_{dri} - \omega_r \lambda_{qri} + (L_m R_r/L_r) i_{ds} \end{aligned} \tag{4}$$

The methodology of the conventional speed estimation approach [2] is briefly described in the following. The voltage model is considered as the reference model, and the current model, which involves the rotor speed information ω_r, is regarded as the adjustable model. If all the parameters and rotor speed employed in these two models are equal to their actual values, the estimated rotor fluxes based on eqns. 3 and 4 will coincide. In practice, a low-pass filter is used instead of pure integration in the realisation of eqns. 3 and 4 to avoid the problems caused by the initial condition offset and drift [3]. Excluding the influence of parameter variations, an estimation error defined by $\varepsilon \triangleq \lambda_{drv}\lambda_{qri} - \lambda_{qrv}\lambda_{dri}$ is derived when the speed used in the current model is not identical to the actual one. A tuning signal for the current model is generated from the regulation of this error through a PI controller. The adaptation mechanism is designed using Popov's hyperstability theory to derive the estimated speed:

$$\hat{\omega}_r = (k_p + k_i/s)\varepsilon \tag{5}$$

We can see from eqns. 3 and 4 that different motor parameters are employed in the V- and I- models in this estimation mechanism. Thus the parameter uncertainties will lead to the contribution to the error ε and result in speed estimation error. Although some research [11–15] has been performed to improve this by on-line estimation of some key parameters, the success is still limited.

In this paper, a speed estimator with parameter uncertainty cancellation is proposed. Configurations of the proposed V-I model speed estimator scheme and the VSS compensation control scheme are shown in Figs. 1*a* and *b*. The control signal generated by the VSS controller is applied for adaptively tuning the R_s used in the speed estimator to cancel the effects of parameter uncertainties.

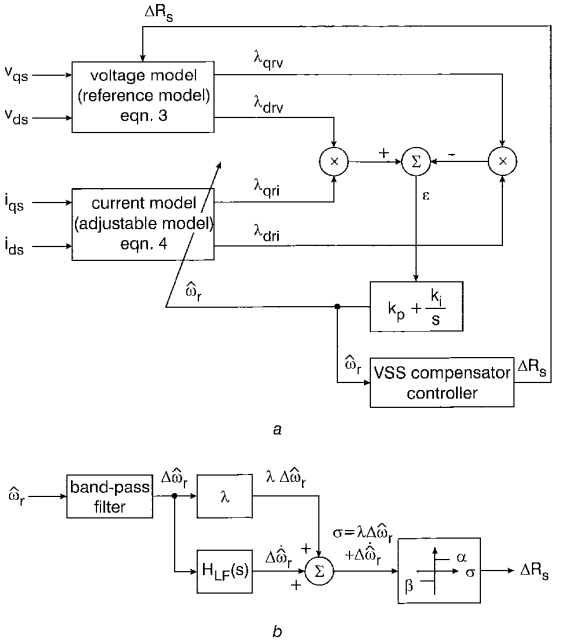

Fig. 1 *Configuration of proposed V-I model speed estimator and VSS compensation control scheme*
a Speed estimator
b Control scheme

3 Parameter sensitivity analysis of V-I model-based MRAC speed estimator

To understand fully the speed estimation errors due to various parameter variations, the parameter sensitivity analysis of the V-I model-based estimator is first studied. The

governing equations in eqns. 3 and 4 are transformed to the synchronous rotating reference frame as:

voltage model:

$$\begin{aligned} p\lambda_{qrv} &= (L_r/L_m)(v_{qs} - R_s i_{qs} - \delta p i_{qs} - \omega_e \delta i_{ds}) \\ &\quad - \omega_e \lambda_{drv} \\ p\lambda_{drv} &= (L_r/L_m)(v_{ds} - R_s i_{ds} - \delta p i_{ds} + \omega_e \delta i_{qs}) \\ &\quad + \omega_e \lambda_{qrv} \end{aligned} \tag{6}$$

current model:

$$\begin{aligned} p\lambda_{qri} &= -(R_r/L_r)\lambda_{qri} + (\omega_e - \omega_r)\lambda_{dri} \\ &\quad + (L_m R_r/L_r) i_{qs} \\ p\lambda_{dri} &= -(R_r/L_r)\lambda_{dri} - (\omega_e - \omega_r)\lambda_{qri} \\ &\quad + (L_m R_r/L_r) i_{ds} \end{aligned} \tag{7}$$

where ω_e is the synchronous electrical angular speed.

In the following parameter sensitivity analysis for the V-I model based speed estimation scheme, the perturbations of the specific parameter and the rotor speed around a chosen operating point are first made with other parameters and variables being kept constant. Then, the transfer function between the error of estimated speed and the parameter change is derived. The coefficients of the numerators and denominators of all transfer functions are listed in the Appendix (Section 8).

3.1 Stator resistance

Initially, the estimated speed $\hat{\omega}_r$ is equal to the real speed ω_r at the operation point, as all parameters are correct. The steady-state values of the rotor flux components have the features $\lambda_{qrvo} = \lambda_{qrio} \triangleq \lambda_{qro}$ and $\lambda_{drvo} = \lambda_{drio} \triangleq \lambda_{dro}$. Assuming that the parameter uncertainty to be studied is stator resistance, the small signals of stator resistance and the resulting rotor flux components in eqns. 6 and 7 are defined as follows:

$$\begin{aligned} &\Delta R_s = R_{so} - R_s \\ &\Delta\lambda_{qrv} = \lambda_{qrvo} - \lambda_{qrv}, \quad \Delta\lambda_{drv} = \lambda_{drvo} - \lambda_{drv} \\ &\Delta\lambda_{qri} = \lambda_{qrio} - \lambda_{qri}, \quad \Delta\lambda_{dri} = \lambda_{drio} - \lambda_{dri} \end{aligned} \tag{8}$$

Linearising the estimated speed $\hat{\omega}_r$ in eqn. 5, we can obtain

$$\begin{aligned} \Delta\hat{\omega}_r = \left(k_p + \frac{k_i}{s}\right) [&\lambda_{qro}(\Delta\lambda_{dri} - \Delta\lambda_{drv}) \\ &- \lambda_{dro}(\Delta\lambda_{qri} - \Delta\lambda_{qrv})] \end{aligned} \tag{9}$$

A transfer function between the estimated speed and the stator resistance changes can be obtained, from eqns. 6–9, to be

$$\frac{\Delta\hat{\omega}_r}{\Delta R_s} = \frac{b_1 s^4 + b_2 s^3 + b_3 s^2 + b_4 s + b_5}{a_1 s^5 + a_2 s^4 + a_3 s^3 + a_4 s^2 + a_5 s + a_6} \tag{10}$$

where the coefficients $a_1 \sim a_6$ and $b_1 \sim b_5$ are defined in the Appendix (Section 8). In the expressions of coefficients, the steady-state values of ω_{eo}, ω_{ro}, i_{qso}, i_{dso}, λ_{qro} and λ_{dro} at the chosen operating point can be found by solving eqns. 2, 6 and 7, with all time derivatives being set equal to zero.

The motor used here has the following characteristics: three-phase, Y-connected, 2-pole, 800W, 2000rpm, 120V/5.4A and has the following nominal parameters obtained from conventional no-load and locked-rotor tests:

$$\begin{aligned} &R_s = 1.1\ \Omega,\ R_r = 1.3\ \Omega \\ &L_s = 0.144\ \text{H},\ L_r = 0.144\ \text{H},\ L_m = 0.136\ \text{H} \end{aligned} \tag{11}$$

Using the parameters listed in eqn. 11 and the chosen operation point (v_{qso}, v_{dso}, ω_{ro}, T_{Lo}), other steady-state variables (ω_{eo}, i_{qso}, i_{dso}, λ_{qro}, λ_{dro}) can be found.

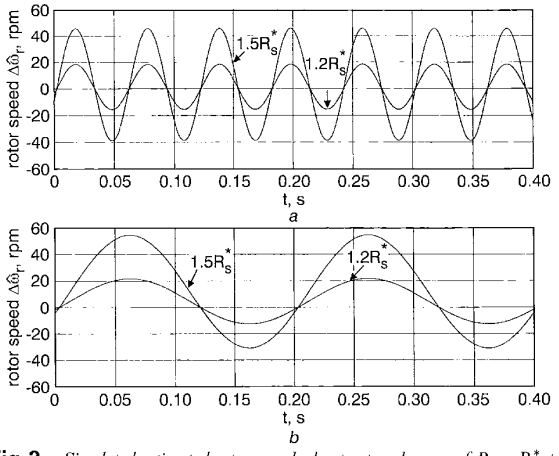

Fig. 2 *Simulated estimated rotor speeds due to step changes of $R_s = R_s^*$ to 1.2 R_s^* and 1.5 R_s^**
a $\hat{\omega}_{ro}$ = 1000rpm
b $\hat{\omega}_{ro}$ = 300rpm

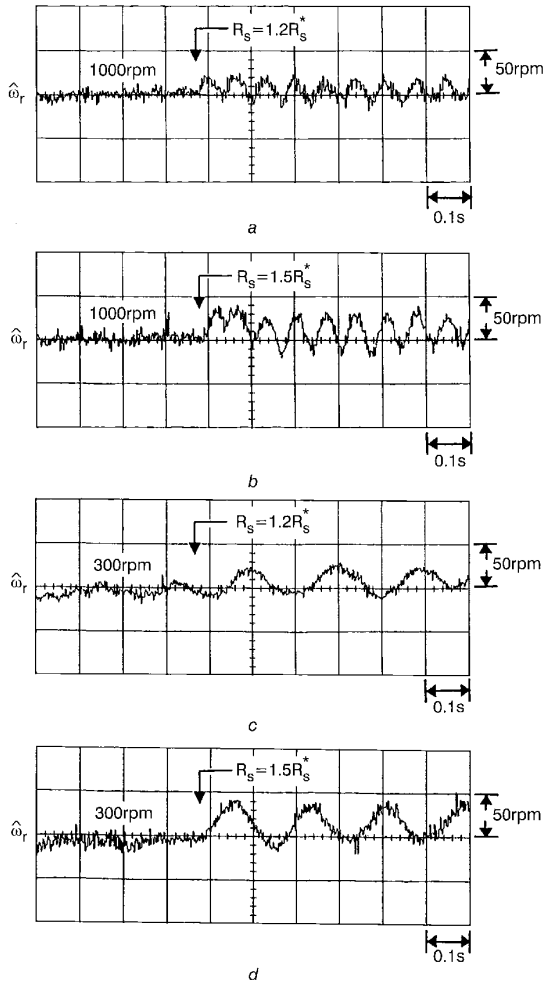

Fig. 3 *Measured estimated rotor speeds due to step changes*
a $R_s = R_s^* \rightarrow 1.2\ R_s^*$ at $\hat{\omega}_{ro}$ = 1000rpm
b $R_s = R_s^* \rightarrow 1.5\ R_s^*$ at $\hat{\omega}_{ro}$ = 1000rpm
c $R_s = R_s^* \rightarrow 1.2\ R_s^*$ at $\hat{\omega}_{ro}$ = 300rpm
d $R_s = R_s^* \rightarrow 1.5\ R_s^*$ at $\hat{\omega}_{ro}$ = 300rpm

With a step stator resistance change from $R_s = R_s^* = 1.1\Omega$ to 1.2 R_s^* and 1.5 R_s^*, the simulated estimated rotor

speeds at the chosen cases (v_{qso} = 60√2V,v_{dso} = 0V, ω_{ro} = 1000rpm, T_{Lo} = 1.7Nm, k_p = 65000, k_i = 50000) and (v_{qso} = 60√2/3.33V, v_{dso} = 0V, ω_{ro} = 300rpm, T_{Lo} = 1.7Nm, k_p = 65000, k_i = 50000) are shown in Figs. 2*a* and *b*, respectively. The results indicate that the stator resistance uncertainty will lead to an oscillatory estimated speed with a small bias, the oscillation frequency is closely related to the excitation frequency ω_{eo}, and the amplitude of oscillation depends on the magnitude of the stator resistance change. Fig. 3 shows the measured estimated speeds under the same conditions as those of Fig. 2. The measured results show that they are very close to those obtained by simulation.

3.2 Rotor resistance

Let the only parameter change be $\Delta R_r = R_{ro} - R_r$; following the same procedure described above, a transfer function between the estimated speed and the rotor resistance changes can also be derived, from eqns. 6–9 to be

$$\frac{\Delta\hat{\omega}_r}{\Delta R_r} = \frac{d_1 s^2 + d_2 s + d_3}{c_1 s^3 + c_2 s^2 + c_3 s + c_4} \tag{12}$$

With a step rotor resistance change from $R_r = R_r^* = 1.3\Omega$ to 1.2 R_r^* and 1.5 R_r^*, the simulated estimated rotor speeds at the same two operating points as those in Fig. 2 are shown in Fig. 4, respectively. The results indicate that the change in R_r only leads to the steady-state error of speed estimation. The measured results under the same conditions, plotted in Figs. 5*a* to *d*, are quite close to the simulation results.

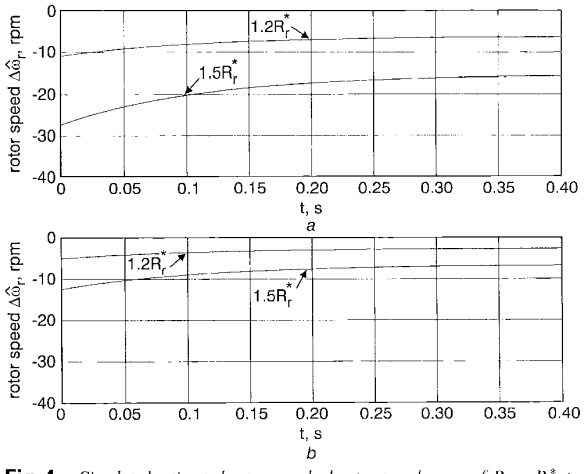

Fig. 4 *Simulated estimated rotor speeds due to step changes of $R_r = R_r^*$ to 1.2 R_r^* and 1.5 R_r^**
a $\hat{\omega}_{ro}$ = 1000rpm
b $\hat{\omega}_{ro}$ = 300rpm

3.3 Stator and rotor leakage inductances

Let $\Delta L_{lr} = L_{lro} - L_{lr}$ and $\Delta L_{ls} = L_{lso} - L_{ls}$, where $L_{lro} = L_{ro} - L_{mo}$ and $L_{lso} = L_{so} - L_{mo}$ denote the nominal stator and rotor leakage inductances. Following the same derivation procedure, the transfer functions between the estimated speed error and the leakage inductance uncertainties can be found to be

$$\frac{\Delta\hat{\omega}_r}{\Delta L_{ls}} = \frac{c_1 s^4 + c_2 s^3 + c_3 s^2 + c_4 s + c_5}{a_1 s^5 + a_2 s^4 + a_3 s^3 + a_4 s^2 + a_5 s + a_6} \tag{13}$$

$$\frac{\Delta\hat{\omega}_r}{\Delta L_{lr}} = \frac{f_1 s^4 + f_2 s^3 + f_3 s^2 + f_4 s + f_5}{a_1 s^5 + a_2 s^4 + a_3 s^3 + a_4 s^2 + a_5 s + a_6} \tag{14}$$

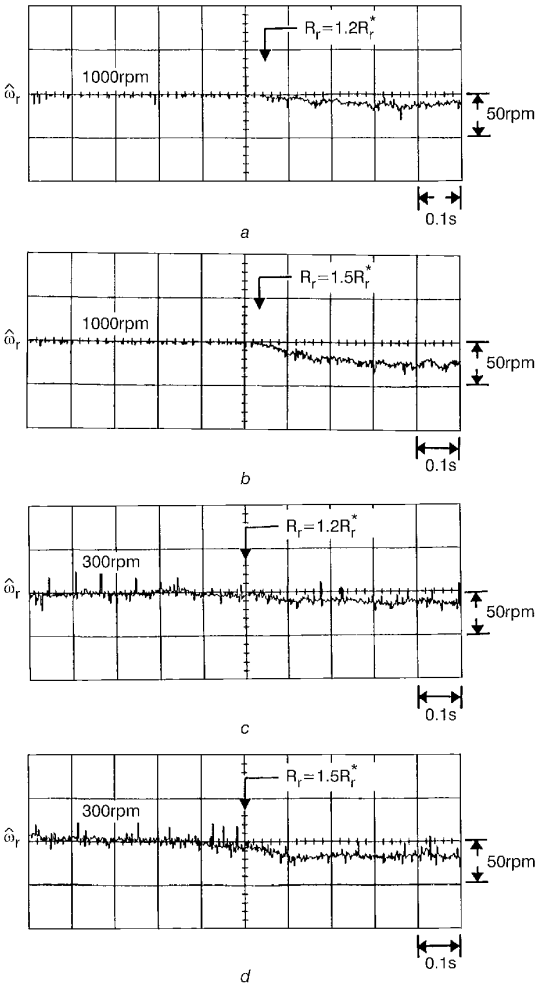

Fig. 5 *Measured estimated rotor speeds due to step changes*
a $R_r = R_r^* \rightarrow 1.2\ R_r^*$ at $\hat{\omega}_{ro}$ = 1000rpm
b $R_r = R_r^* \rightarrow 1.5\ R_r^*$ at $\hat{\omega}_{ro}$ = 1000rpm
c $R_r = R_r^* \rightarrow 1.2\ R_r^*$ at $\hat{\omega}_{ro}$ = 300rpm
d $R_r = R_r^* \rightarrow 1.5\ R_r^*$ at $\hat{\omega}_{ro}$ = 300rpm

The simulated rotor speed variations due to the stator leakage inductance changes, from $L_{ls} = L_{ls}^*$ to 1.2 L_{ls}^* and 1.5 L_{ls}^*, and the rotor leakage inductance changes, from $L_{lr} = L_{lr}^*$ to 1.2 L_{lr}^* and 1.5 L_{lr}^*, are shown in Figs. 6*a* to *d*. The results indicate that the nature of the estimated speed errors due to leakage inductance uncertainties is the same as that of stator resistance change. Figs. 7*a* and *b* show the measured estimated speed variations when stator and rotor leakage inductances are changed simultaneously from $L_{ls} = L_{ls}^*$ to 1.2 L_{ls}^* and $L_{lr} = L_{lr}^*$ to 1.2 L_{lr}^* at $\hat{\omega}_{ro}$ = 1000rpm and 300rpm, respectively.

3.4 Magnetising inductance

Similarly, the transfer function between the estimated speed error and the magnetising inductance change can be derived, from eqns. 6–9, to be

$$\frac{\Delta\hat{\omega}_r}{\Delta L_m} = \frac{L_{mo}}{L_{ro}} \frac{g_1 s^4 + g_2 s^3 + g_3 s^2 + g_4 s + g_5}{a_1 s^5 + a_2 s^4 + a_3 s^3 + a_4 s^2 + a_5 s + a_6} \tag{15}$$

With a step magnetising inductance change from $L_m = L_m^*$ to 1.2 L_m^* and 1.5 L_m^*, the simulated and measured estimated rotor speeds at the two chosen operating conditions are shown in Figs. 8 and 9, respectively. The results show

that the errors due to the variation in magnetising inductance have the same dynamic behaviour as those of stator resistance, but with smaller magnitudes.

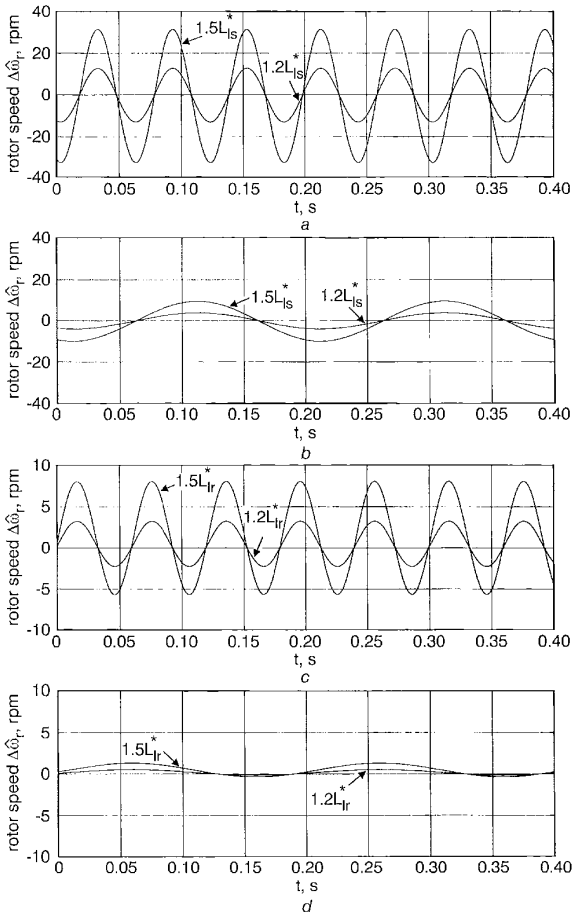

Fig. 6 *Simulated estimated rotor speeds due to step changes*
a $L_{ls} = L_{ls}^*$ to 1.2 L_{ls}^* and 1.5 L_{ls}^* at $\hat{\omega}_{ro}$ = 1000rpm
b $L_{ls} = L_{ls}^*$ to 1.2 L_{ls}^* and 1.5 L_{ls}^* at $\hat{\omega}_{ro}$ = 300rpm
c $L_{lr} = L_{lr}^*$ to 1.2 L_{lr}^* and 1.5 L_{lr}^* at $\hat{\omega}_{ro}$ = 1000rpm
d $L_{lr} = L_{lr}^*$ to 1.2 L_{lr}^* and 1.5 L_{lr}^* at $\hat{\omega}_{ro}$ = 300rpm

3.5 Observations

Some key features of the V-I model-based speed estimator can be deduced from the above error analyses:

(*a*) All the speed error transfer functions except those of rotor resistance uncertainty have the same characteristic equation. The simulation and measured results also show that they have the same type of estimated speed error dynamics. The rotor resistance uncertainty only leads to the steady-state error in the estimated speed.

(*b*) The lower the speed, the more prominent the effects of parameter variations. Fig. 10 summarises the normalised errors of various parameter changes at rotor speed = 300rpm. It is obvious from the comparison that the dominant parameter in this type of speed estimation approach is the stator resistance. The possible parameter variation ranges of an induction motor will be $1.0 \leq R_r/R_r^* \leq 1.5$, $1.0 \leq R_s/R_s^* \leq 1.5$, $0.8 \leq L_m/L_m^* \leq 1.2$, and the variations in leakage inductances are negligibly small. As the variations in leakage inductances and magnetising inductance have the same type of error dynamics as those of stator resistance, but with much smaller values, their effects on speed estimation can be compensated by tuning the stator resistance through the proposed control approach.

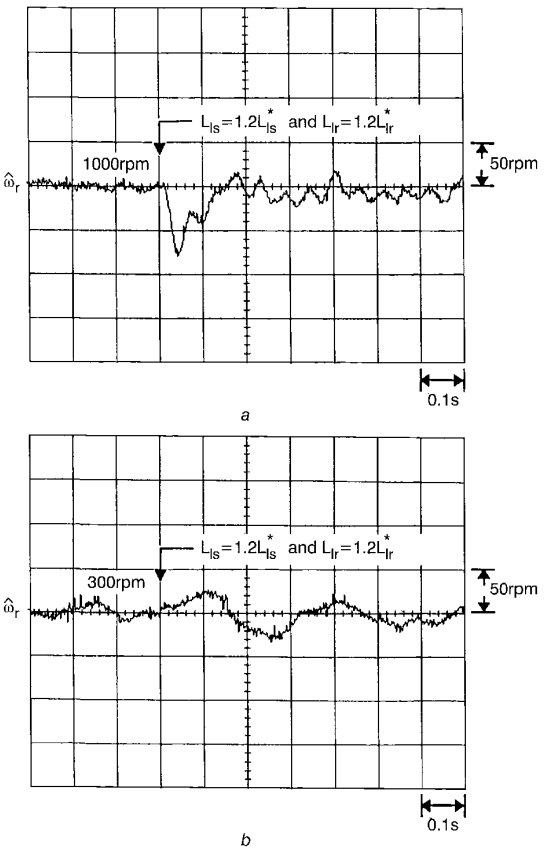

Fig. 7 *Measured estimated speeds due to step changes of* $L_{ls} = L_{ls}^*$ *to 1.2* L_{ls}^* *and* $L_{lr} = L_{lr}^*$ *to 1.2* L_{lr}^*
a $\hat{\omega}_{ro}$ = 1000rpm
b $\hat{\omega}_{ro}$ = 300rpm

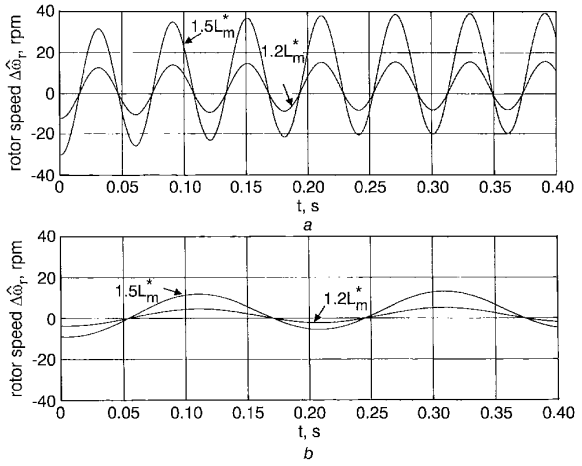

Fig. 8 *Simulated estimated speeds due to step change of* $L_m = L_m^*$ *to 1.2* L_m^* *and 1.5* L_m^*
a $\hat{\omega}_{ro}$ = 1000rpm
b $\hat{\omega}_{ro}$ = 300rpm

4 Proposed uncertainty cancellation approach

The parameter sensitivity analyses made in the preceding Section indicate that both AC and/or DC speed estimation error signals exist, owing to the parameter uncertainties. The transient speed error will be reduced by the proposed uncertainty cancellation approach. In the proposed approach, the AC error signal is extracted and used as the input of a VSS control scheme.

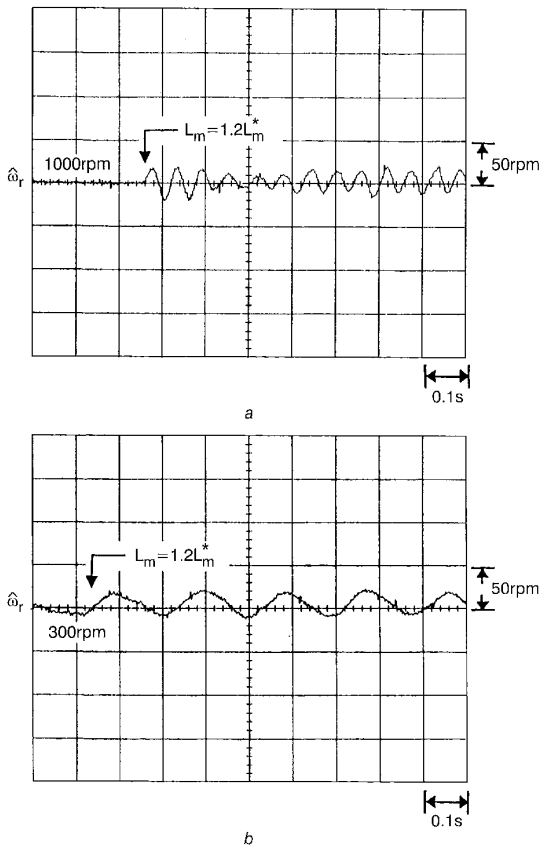

Fig. 9 *Measured estimated speeds due to step change of $L_m = L_m^*$ to 1.2 L_m^**
a $\hat{\omega}_{ro}$ = 1000rpm
b $\hat{\omega}_{ro}$ = 300rpm

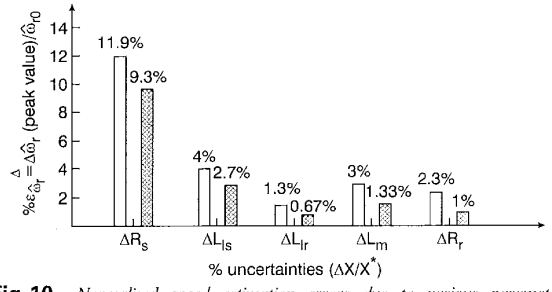

Fig. 10 *Normalised speed estimation errors due to various parameter changes at $\hat{\omega}_{ro}$ = 300rpm*
□ $\Delta x/\Delta x^*$ = 0.5; ■ $\Delta x/\Delta x^*$ = 0.2

4.1 VSS control law

In the VSS control scheme shown in Fig. 2, the transient speed estimation error $\Delta\hat{\omega}_r$ is extracted from $\hat{\omega}_r$ using a band-pass filter, and it is used as the input of the VSS controller. The sliding line equation is defined as

$$\sigma = \lambda\Delta\hat{\omega}_r + \Delta\dot{\hat{\omega}}_r \tag{16}$$

and the compensation signal for tuning the stator resistance is set to be

$$\Delta R_s = \begin{cases} \alpha\ \Omega & \Delta\hat{\omega}_r\sigma \geq 0 \\ \beta\ \Omega & \Delta\hat{\omega}_r\sigma < 0 \end{cases} \tag{17}$$

To avoid undesirable high-frequency noise amplification due to a pure differentiator, a low-pass filter is used to obtain the observed value of the speed derivative

$$H_{LP}(s) = \frac{s}{(1+\mu_1 s)(1+\mu_2 s)} \tag{18}$$

Although $H_{LP}(s)$ serves as a differentiator within the dynamic frequency range, it will become a low-pass filter for high-frequency noises.

4.2 Simulation and experimental results

The configuration of an IFO induction motor drive with the proposed speed estimator is shown in Fig. 11. The switched load resistance R_L of the DC generator is employed to change the dynamic load of the induction motor. The parameters of the proposed VSS compensation scheme listed in eqns. 16–18 are set to be

$$\lambda = 1,\ \alpha = 0.6,\ \beta = -0.6 \tag{19}$$

$$H_{LP}(s) = \frac{s}{0.225s^2 + 0.3s + 1} \tag{20}$$

where, considering the compromise between the slowly changing property of stator resistance and the high-frequency noise rejection, the cutoff frequency of the low-pass filter part of $H_{LP}(s)$ is set to be 0.5Hz. For the nominal value of $R_s^* = 1.1\Omega$ and the chosen parameters $\alpha = 0.6$ and $\beta = -0.6$, the tuning range of R_s is $0.5\Omega \sim 1.7\Omega$, which covers its typical variation range ($1.0 \leq R_s/R_s^* \leq 1.5$). As for the parameter of $\lambda = 1$, it is determined using a trial-and-error approach. For the chosen parameters listed in eqns. 19 and 20, the successful VSS control operation can be confirmed from the simulated and measured results.

The simulated rotor speed $\hat{\omega}_r$ of the IFO induction motor drive, before and after applying the proposed speed estimator due to the changes in the stator resistance (R_s = 1.0 R_s^* to 1.2 R_s^*), the leakage inductances (L_{ls} = 1.0 L_{ls}^* and L_{lr} = 1.0 L_{lr}^* to 1.2 L_{ls}^* and 1.2 L_{lr}^*) and the magnetising inductance (L_m = 1.0 L_m^* to 1.2 L_m) at ($\hat{\omega}_{ro}$ = 300 rpm, T_{Lo} = 1.7Nm), are plotted in Figs. 12*a* to *c*. The results clearly indicate that the oscillating speed ripples have been greatly reduced by the proposed speed estimator.

The designed speed estimation algorithms are realised using C-language on a PC 486-based control computer with necessary interfacing cards. The measured rotor speed $\hat{\omega}_r$ of the IFO induction motor drive, before and after applying the proposed speed estimator due to the changes in the stator resistance (R_s = 1.0 R_s^* to 1.2 R_s^*), the leakage inductance (L_{ls} = 1.0 L_{ls}^* and L_{lr} = 1.0 L_{lr}^* to 1.2 L_{ls}^* and 1.2 L_{lr}^*) and the magnetising inductance (L_m = 1.0 L_m^* to 1.2 L_m) at ($\hat{\omega}_{ro}$ = 300rpm, T_{Lo} =1.7Nm, R_{Lo} = 77.6Ω) are plotted in Figs. 13*a* to *c*. The results are very close to those obtained by simulation and further confirm the effectiveness of the proposed speed estimation approach.

5 Robust speed control

5.1 Dynamic model

For the IFO induction motor drive using the proposed speed estimate as feedback signal, three kinds of dynamic model uncertainty exist, namely, non-ideal field orientation, inaccurate speed estimation and variations in motor and mechanical load parameters. To account for these effects, the dynamic behaviour of the motor drive shown in Fig. 11 is reasonably represented by the transfer function block diagram shown in Fig. 14, wherein the proposed controllers are also shown. The major constituent parts are briefly described as follows:

5.1.1 Motor drive model:

$k_t \triangleq \frac{3}{4}P(L_m^2/L_r)i_{ds}^*$: torque generating constant of an ideal IFO induction motor drive

$\Delta_t(s)$: the torque generation unmodelled dynamic due to non-ideal field orientation [21]

$\bar{J}$: nominal total mechanical inertia

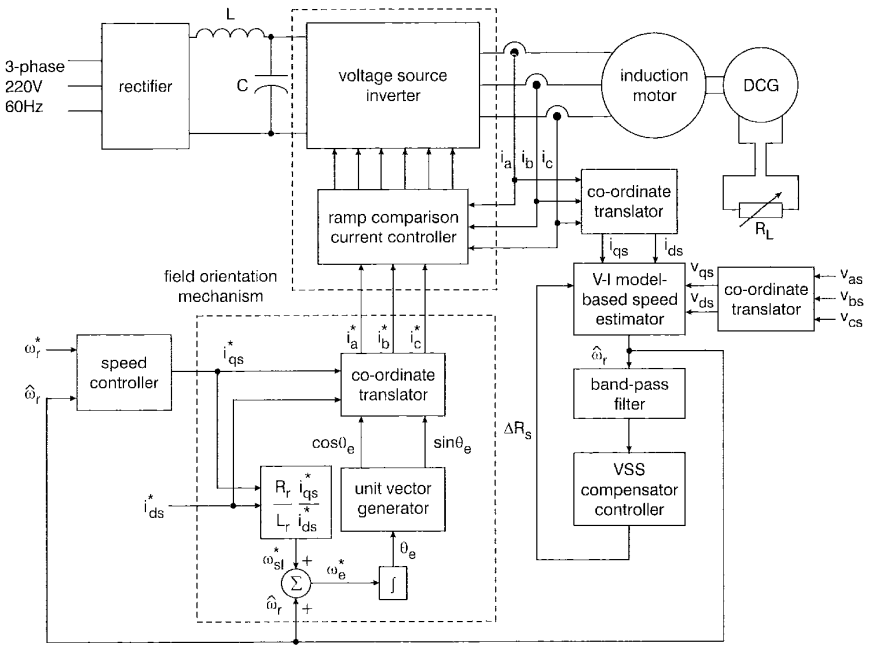

Fig. 11 *Speed sensorless IFO induction motor drive with the proposed speed estimator*

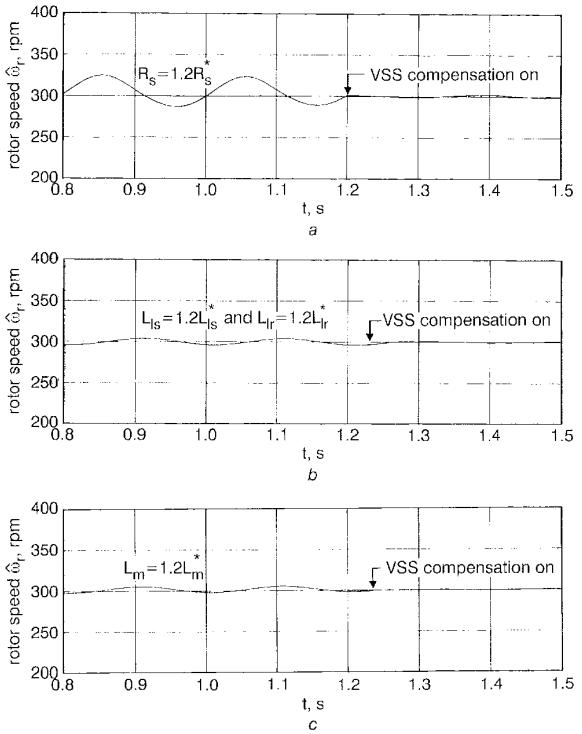

Fig. 12 *Simulated rotor speeds of the IFO induction motor drive before and after applying proposed speed estimator*
$\hat{\omega}_{ro}$ = 300rpm, T_{Lo} = 1.7Nm
Step changes of
a R_s = 1.0 R_s^* to 1.2 R_s^*
b L_{ls} = 1.0 L_{ls}^* to 1.2 L_{ls}^* and L_{lr} =1.0 L_{lr}^* to 1.2 L_{lr}^*
c L_m = 1.0 L_m^* to 1.2 L_m^*

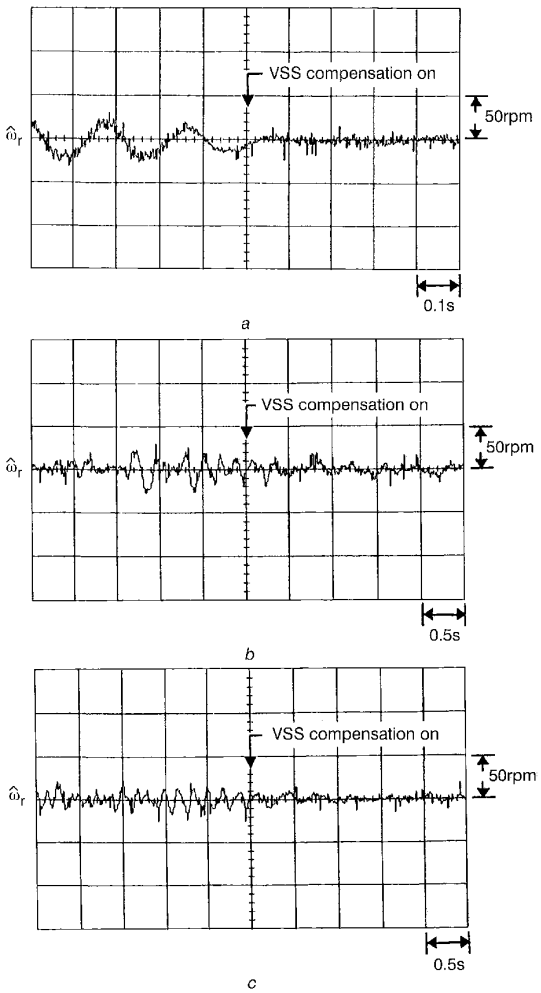

Fig. 13 *Measured rotor speeds*
$\hat{\omega}_{ro}$ = 300rpm, T_{Lo} = 1.7Nm
Step changes of
a R_s = 1.0 R_s^* to 1.2 R_s^*
b L_{ls} = 1.0 L_{ls}^* to 1.2 L_{ls}^* and L_{lr} =1.0 L_{lr}^* to 1.2 L_{lr}^*
c L_m = 1.0 L_m^* to 1.2 L_m^*

$\bar{B}$: nominal total damping coefficient

$\Delta G_p(s) \triangleq 1/(Js + B) - 1/(Js + \bar{B})$: mechanical uncertainty model

$e^{-\tau_d s}$: transport delay, which is mainly caused by the speed estimation

$\hat{k}_{\omega r}$: nominal estimation speed conversion constant

$\Delta_k(s)$: estimation speed uncertainty model

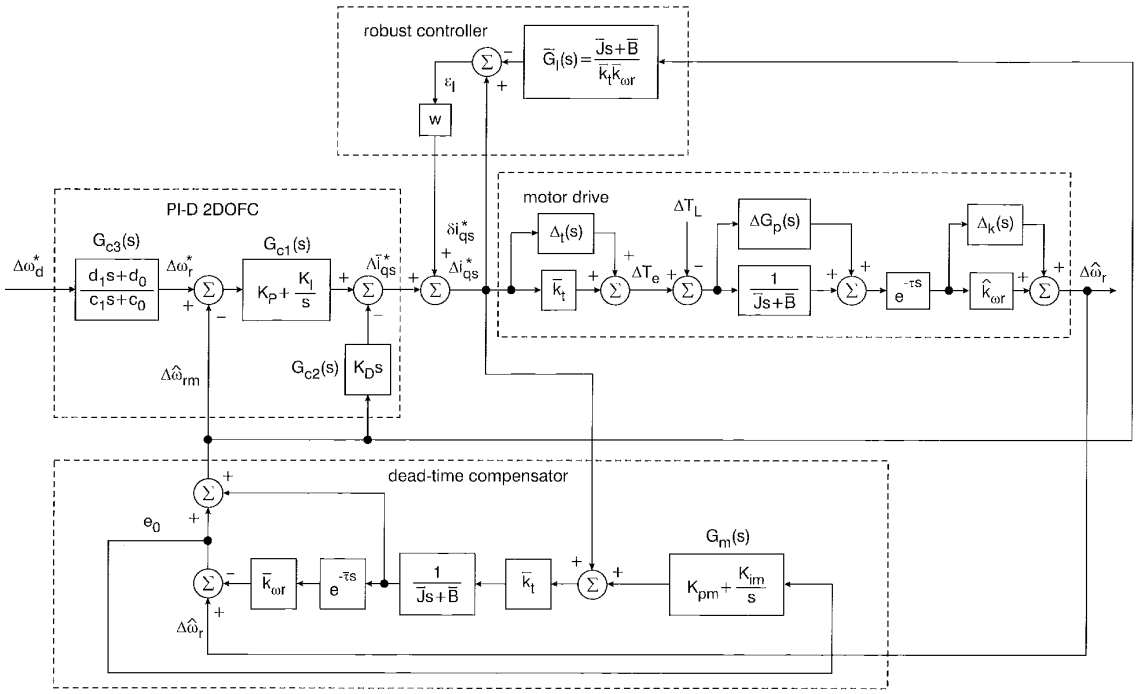

Fig. 14 *Block diagram of proposed robust PI-D 2DOF controller*

where $\Delta_k(s)$ represents the dynamic and static errors of the proposed speed estimator. $\hat{k}_{\omega r}$ and $\Delta_k(s)$ are not constant and depend on the nature of the parameter variations and the compensation control characteristics of the proposed method.

5.1.2 Controllers:

(*a*) PI-D 2DOFC: at a chosen nominal operating condition, the PI-D 2DOFC is designed according to the estimated linear motor drive model and the given command tracking and load regulation control specifications.

(*b*) Robust controller: a model error ε_I is extracted out the nominal inverse linear plant model, and a compensation signal δi_{qs}^* is generated to reduce the performance degradation due to inaccurate speed estimation, non-ideal field-orientation and motor drive model parameter variations.

(*c*) Dead-time compensator: it is known that the dead-time element is a very difficult control non-linearity, particularly for the speed sensorless motor drive, as the dead-time will be much enlarged due to the feedback of estimated speed. The dead-time compensator [19] is employed here to let the dead-time be equivalently moved outside the closed-loop, and, hence, the stability and dynamic control performance are greatly enhanced.

The motor drive model is difficult to obtain accurately through physical derivation. Thus, let the feedback controller $G_{c1}(s) = K_p$ (P-type) and other controllers be disabled, and the IFO induction motor drive be operated using the estimated speed as feedback signal. The motor drive model parameters are estimated at the chosen nominal operation condition ($\hat{\omega}_{ro}$ = 1000 rpm, R_{Lo} = 77.6Ω) using the step response approach [16] to be $\bar{k}_t$ = 0.6358, $\bar{\tau}$ = 0.04s, $\bar{a}$ = 0.7937 and $\bar{b}$ = 117.65. Then, from the above definitions, we can find that $\bar{J}$ = 0.0085001N·m·s^2 and $\bar{B}$ = 0.0067466N·m·s/rad. According to scaling set in this experimental drive (1V = 1000rpm = 104.7rad/s, i.e. $\bar{k}_{\omega r}$ = 0.00955V·s/rad), $\bar{J}$ and $\bar{B}$ can also be represented as $\bar{J}$ = 0.89007N·m·s·rad/V and $\bar{B}$ = 0.70645N·m/V, respectively.

5.2 Controller design

5.2.1 PI-D 2DOF controller: At the design stage, let all the uncertainty models and nonlinearities in Fig. 14 be neglected. The speed control specifications are given below:

Step command tracking response ($\Delta\omega_d^*$ = 100rpm):

(i) Response time t_{re} = 0.2s, which is defined as the time that the response rises from zero to 90% of its final value.

(ii) Overshoot = 0.

(iii) Steady-state error = 0.

(iv) Maximum value of control force Δi_{qsm}^* = 3.5A.

Step load regulation response (ΔT_L = 1N·m):

(*a*) Maximum dip $\Delta\omega_{dm}$ = 30rpm.

(*b*) Steady-state error = 0.

The governed equations concerning the controller parameters and the given specifications have been derived in [17]. Using the nominal linear plant model, the PI-D 2DOF controller designed to meet the given specifications is found to be

$$K_P = 39.562,\ K_I = 292.6869,\ K_D = 0.3949$$
$$c_0 = 291.2322,\ c_1 = 39.9181$$
$$d_0 = 291.2322,\ d_1 = 17.0655 \qquad (21)$$

5.2.2 Robust controller: In real operation, the actual plant parameters can deviate significantly from the nominal ones used in the design of the speed estimator and controller, and then the speed dynamic response will worsen. To improve this, a simple RC is employed here. The inverse model used to extract the model error is

$$\bar{G}_I(s) = \frac{\bar{J}s + \bar{B}}{\bar{k}_t\bar{k}_{\omega r}} \qquad (22)$$

and the weighting factor w, $0 < w < 1$, is chosen to make the compromise between the desired control performance, control stability and control effort [19]. The closer w approaches 1, the better the control performance achieved,

but the the resulting closed-loop control system becomes unstable more easily. The major factor to be considered is the dead-time element. The analysis of performance improvement by this type of robust control can be referred to in [19].

5.3 Dead-time compensator

The major purpose of the dead-time compensator is to let the dead-time element be equivalently placed outside the closed-loop, and thus its effect on stability can be much reduced. The simple PI controller $G_{pi}(s)$ is adopted here to eliminate the model error e_0 as quickly as possible and thus to improve the performance of the dead-time compensator. The parameters are chosen by trial-and-error, with the help of simulations, to be

$$K_{pm} = 5, \quad K_{im} = 10 \tag{23}$$

5.4 Experimental results

To verify the effectiveness of the proposed speed estimator and robust controller, a mass of 3.78kg (ΔJ = 1.04009 N·m·s·rad/V) is added to the rotor shaft to let $J = \bar{J}$ = 0.89007N·m·s·rad/V be changed to J = 1.93016N·m·s·rad/V ($J \approx 2.2\ \bar{J}$), and the stator resistance used in the proposed speed estimator is intentionally set as $R_s = 1.5\ R_s^*$ (R_s^* = 1.1Ω listed in eqn. 11). Let the motor drive shown in Fig. 11 be operated at 300rpm (R_{Lo} = 77.6Ω), with the proposed robust PI-D 2DOF controller but without the proposed sensorless VSS uncertainty compensation controller. The measured rotor speeds and torque currents of the motor drive due to the command change from 300rpm to 400rpm and load resistance change from R_L = 77.6Ω to 22Ω ($\hat{\omega}_{ro}$ = 300rpm) are plotted in Figs. 15*a* and *b*, respectively. Under the same conditions, the measured results of the motor drive with the designed RC (w = 0.8) and uncertainty cancellation approach in the speed estimator are shown in Figs. 16*a* and *b*. The results shown in Figs. 15 and 16 show that better tracking and regulation control responses are obtained by the proposed approaches.

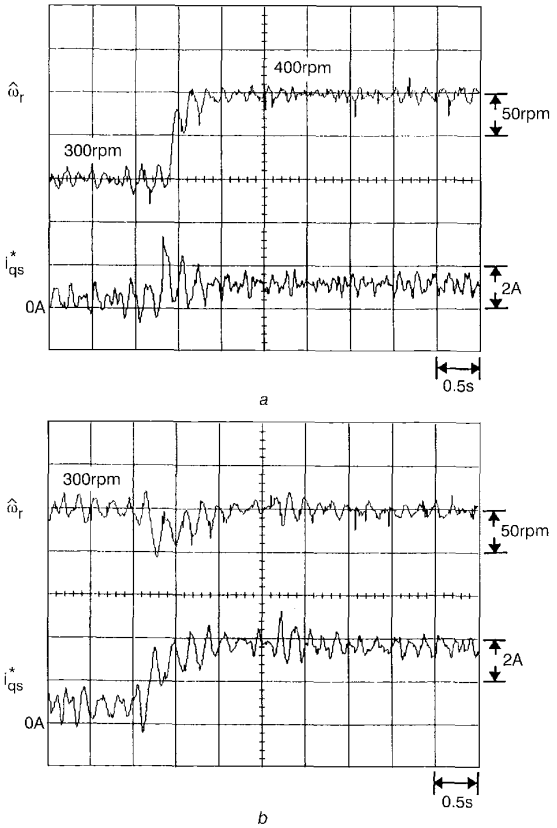

Fig. 15 *Measured rotor speeds and torque currents without the proposed uncertainty cancellation approach (with dead-time compensator and RC) at R_s = 1.5 R_s^* and $J \approx 2.2\ \bar{J}$*
a Step command change from 300rpm to 400rpm (R_L = 77.6Ω)
b Step load resistance change from R_L = 77.6Ω to 22Ω ($\hat{\omega}_{ro}$ = 300rpm)

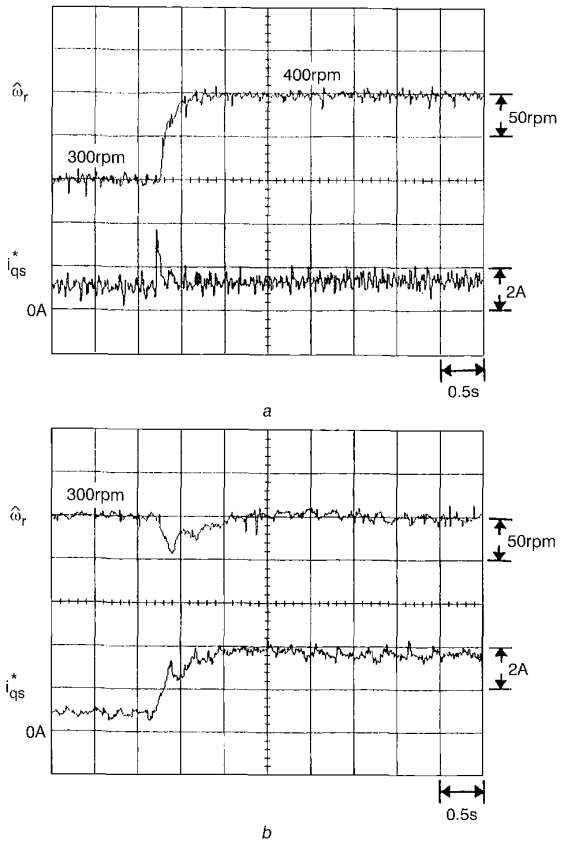

Fig. 16 *Proposed uncertainty cancellation approach*
a Step command change from 300rpm to 400rpm (R_L = 77.6Ω)
b Step load resistance change from R_L = 77.6Ω to 22Ω ($\hat{\omega}_{ro}$ = 300rpm)

For further testing the effectiveness of the dead-time compensator and RC, Fig. 17 shows the measured step speed tracking responses at $J = \bar{J}$ and $R_s = 1.5\ R_s^*$, without and with the designed dead-time compensator (with uncertainty cancellation and without RC). The results indicate that, without adding the dead-time compensator, the response becomes oscillatory. Now let the uncertainty cancellation and dead-time compensation be added; the measured results at $J \approx 2.2\ \bar{J}$ and $R_s = 1.5\ R_s^*$ without and with RC are plotted in Figs. 18 and 19, respectively. Better responses, both in tracking and regulation, yielded by adding the RC can be seen from the results. Real operations indicate that the IFO motor drive with the proposed speed estimator and robust speed controller can be stably operated down to about 100rpm. The measured rotor speeds and torque currents of the motor drive due to command change from 100rpm to 150rpm and load resistance change from R_L = 77.6Ω to 22Ω ($\hat{\omega}_{ro}$ = 100rpm) are plotted in Figs. 20*a* and *b*, respectively. Stable operation below 100rpm is possible, provided that the circuit realisation is improved.

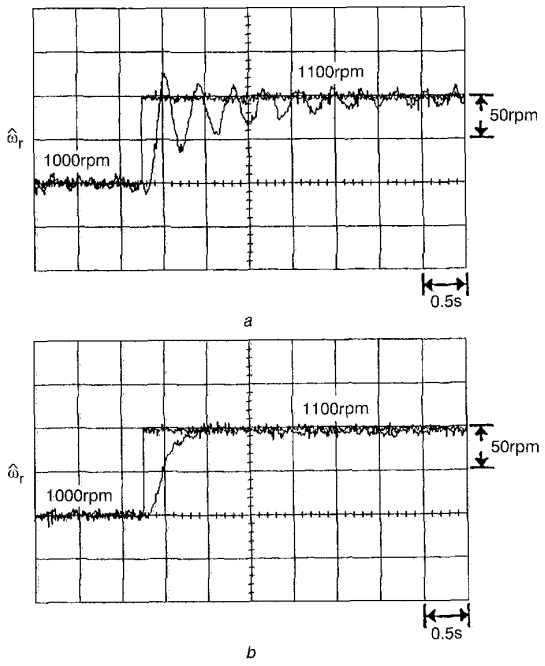

Fig. 17 *Measured rotor speeds due to step command change from 1000 rpm to 1100rpm (R_L = 77.6Ω) at R_s = 1.5 R_s^* and J = J with uncertainty cancellation and without RC*
a Without dead-time compensator
b With dead-time compensator

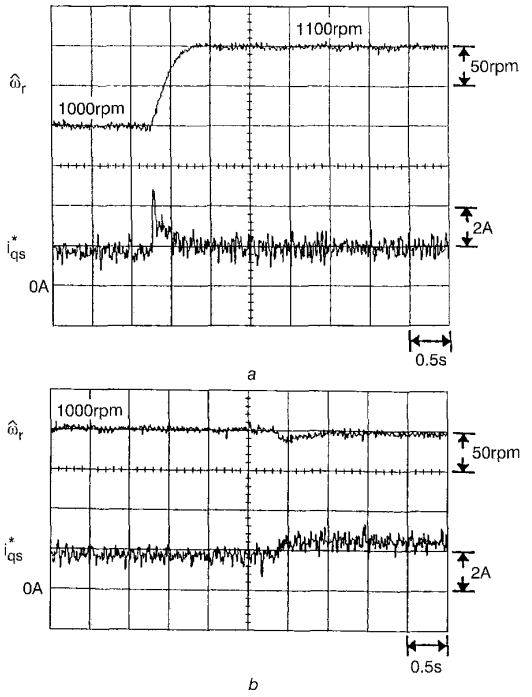

Fig. 19 *Measured rotor speeds and torque currents with RC (with dead-time compensator and uncertainty cancellation) at R_s =1.5 R_s^* and J ≈ 2.2 J*
a Step command change from 1000rpm to 1100rpm (R_L = 77.6Ω)
b Step load resistance change from R_L = 77.6Ω to 52.3Ω ($\hat{\omega}_{ro}$ = 1000rpm)

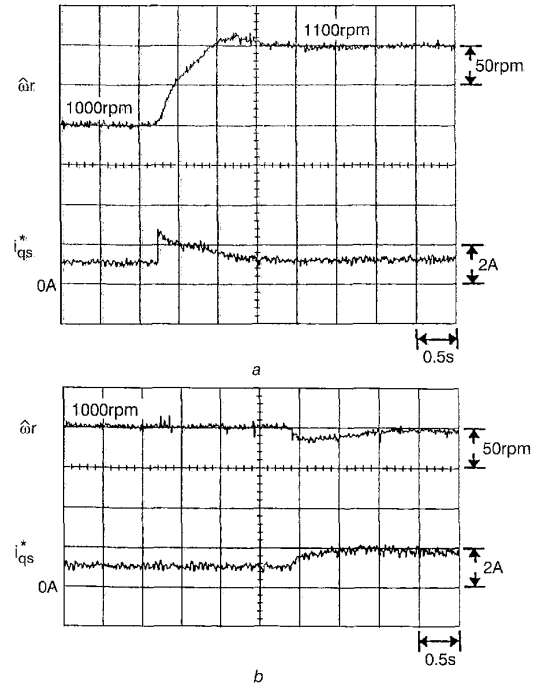

Fig. 18 *Measured rotor speeds and torque currents without RC (with dead-time compensator and uncertainty cancellation) at R_s =1.5 R_s^* and J ≈ 2.2 J*
a Step command change from 1000rpm to 1100rpm (R_L = 77.6Ω)
b Step load resistance change from R_L = 77.6Ω to 52.3Ω ($\hat{\omega}_{ro}$ = 1000rpm)

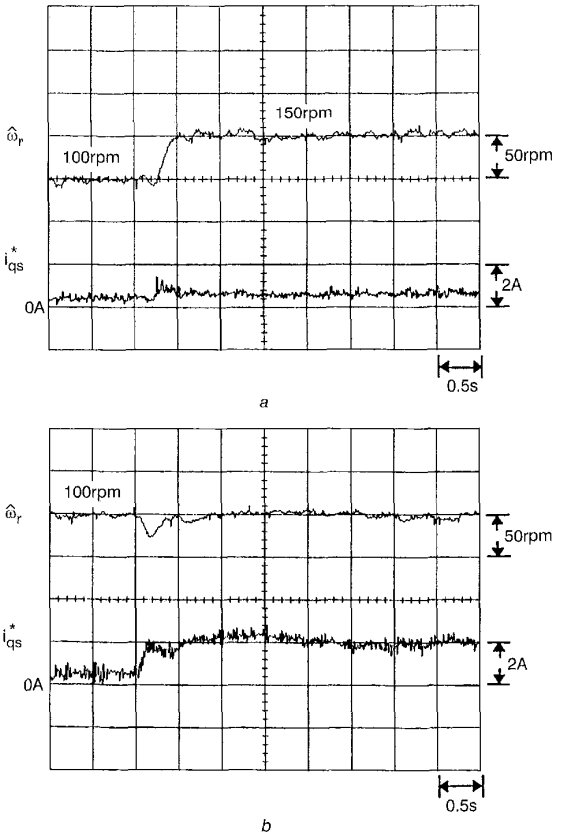

Fig. 20 *Measured rotor speeds and torque currents with the proposed uncertainty cancellation approach (with dead-time compensator and RC) at R_s = 1.5 R_s^* and J ≈ 2.2 J*
a Step command change from 100rpm to 150rpm (R_L = 77.6Ω)
b Step load resistance change from R_L = 77.6Ω to 22Ω ($\hat{\omega}_{ro}$ = 100rpm)

6 Conclusions

Research into the performance improvements of a V-I model-based speed estimator and its application to an IFO motor drive has been presented. The speed estimation errors of the V-I model-based speed estimator due to vari-

ous motor parameter variations are first thoroughly analysed. Based on sensitivity-analysis results, a VSS-based compensation scheme is devised to cancel the effects of parameter uncertainties on the speed estimation performance.

The simulation and measured results have confirmed the effectiveness of the sensitivity analysis and the proposed compensation approaches. For an IFO induction motor drive using the estimated speed as a feedback signal, the decoupling characteristics can be further deteriorated, and the equivalent system dead-time will be enlarged. This will lead to difficulty in achieving a good speed dynamic response.

In this paper, a robust PI-D 2DOF controller with dead-time compensation is designed to let the drive system achieve good dynamic responses, both in step command tracking and load regulating characteristics. A PI-D 2DOF controller is first designed to meet the given control specifications for a nominal case and the estimated linear motor drive model. Then, a robust controller accompanied by a dead-time compensator is added to reduce the effects of parameter variations and system dead-time on the control performance. The experimental results indicate that good control performances in command tracking and load regulation of the sensorless IFO induction motor drive are achieved by the proposed controller when the parameter variations occur.

7 References

1 RAJASHEKARA, K., KAWAMURA, A., and MATSUE, K.: 'Sensorless control of AC motor drives: speed and position sensorless operation' (IEEE Press, New York, 1996)

2 TAMAI, S., SUGIMOTO, H., and YANO, M.: 'Speed sensor-less vector control of induction motor with model reference adaptive system'. IEEE Ind. Appl. Soc. Ann. Meet., IAS'87, 1987, pp. 189–195

3 SCHAUDER, C.: 'Adaptive speed identification for vector control of induction motors without rotational transducers', *IEEE Trans. Ind. Appl.*, 1992, **28**, (5), pp. 1054–1061

4 GRIVA, G., PROFUMO, F., ILAS, C., MAGUERANU, R., and VRANKA, P.: 'A unitary approach to speed sensorless induction motor field oriented drives based on various model reference schemes'. IEEE Ind. Appl. Soc. Ann. Meet., IAS'96, 1996, pp. 1594–1599

5 LEVI, E., and WANG, M.: 'Impact of parameter variations on speed estimation in sensorless rotor flux oriented induction machines'. Proceedings of Power Electron. and Variable Speed Drives conference, 1998, pp. 305–310

6 BLASCO-GIMENEZ, R., ASHER, G.M., SUMNER, M., and BRADLEY, K.J.: 'Dynamic performance limitation for MRAS based sensorless induction motor drives. Part 1: Stability analysis for the closed loop drive', *IEE Proc. Electr. Power Appl.*, 1996, **143**, (2), pp. 113–122

7 ARMSTRONG, G.J., ATKINSON, D.J., and ACARNLEY, P.P.: 'A comparison of estimation techniques for sensorless vector controlled induction motor drive'. Proceedings of EPE'97, Trondheim, Norway, 1997, pp. 1.424–1.429

8 JANSEN, P.L., and LORENZ, R.D.: 'Accuracy limitations of velocity and flux estimation in direct field oriented induction machines'. Proceedings of EPE'93, Brighton, UK, 1993, pp. 312–318

9 MARWALI, M.N., and KEYHANI, A.: 'A comparative study of rotor flux based MRAS and back EMF based MRAS speed estimators for speed sensorless vector control of induction machines'. IEEE Ind. Appl. Soc. Ann. Meet., IAS'97, 1997, pp. 160–166

10 WANG, M., and LEVI, E.: 'Evaluation of steady-state and transient behaviour of a MRAS based sensorless rotor flux oriented induction machine in the presence of parameter detuning', *Electr. Mach. Power Syst.*, 1999, **27**, (11), pp. 1171–1190

11 KUBOTA, H., and MATSUSE, K.: 'Speed sensorless field-oriented control of induction motor with rotor resistance adaptation', *IEEE Trans. Ind. Appl.*, 1994, **30**, (5), pp. 1219–1224

12 ZHEN, L., and XU, L.: 'Sensorless field orientation control of induction machine based on mutual MRAS scheme', *IEEE Trans. Ind. Electron.*, 1998, **45**, (5), pp. 824–831

13 BLASCO-GIMENEZ, R., ASHER, G.M., SUMNER, M., and BRADLEY, K.J.: 'Dynamic performance limitation for MRAS based sensorless induction motor drives. Part 2: Online parameter tuning and dynamic performance studies', *IEE Proc. Electr. Power Appl.*, 1996, **143**, (2), pp. 123–134

14 SILVINO, J.L., RITTER, M.C., and DE RESENDE, P.: 'Sensorless rotor time-constant and mutual inductance estimation for induction motor drive system'. Proceedings of the IEEE international symposium on *Industrial electronics*, IECON'97, 1997, pp. 1060–1064

15 KANMACHI, T., and TAKAHASHI, I.: 'Sensorless speed control of an induction motor with no influence of resistance variation', *Proc. Power Conversion*, 1997, **1**, pp. 91–96

16 LIAW, C.M.: 'System parameter estimation from sampled data', *Control Dyn. Syst.*, 1994, **63**, pp. 161–175

17 LIAW, C.M., CHEN, Y.K., CHAO, K.H., and CHEN, H.C.: 'Quantitative design and implementation of PI-D controller with model-following response for motor drive', *IEE Proc. Electr. Power Appl.*, 1998, **145**, (2), pp. 98–104

18 HSIA, T.C.: 'A new technique for robust control of servo system', *IEEE Trans. Ind. Electron.*, 1989, **36**, (1), pp. 1–7

19 LIAW, C.M., and LIN, F.J.: 'Control of indirect field-oriented induction motor drives considering the effects of dead-time and parameter variations', *IEEE Trans. Ind. Electron.*, 1993, **40**, (5), pp. 486–495

20 BOSE, B.K.: 'Power electronics and AC drives' (Prentice-Hall, 1986)

21 NOVOTNY, D.W., and LIPO, T.A.: 'Vector control and dynamics of AC drives' (Oxford, Clarendon Press, 1996)

8 Appendix

The transfer functions, which are derived in Section 3, representing the dynamic characteristics of estimated speed errors for all parameter changes are listed as follows:

8.1 Stator resistance

$$\frac{\Delta\hat{\omega}_r}{\Delta R_s} = \frac{b_1 s^4 + b_2 s^3 + b_3 s^2 + b_4 s + b_5}{a_1 s^5 + a_2 s^4 + a_3 s^3 + a_4 s^2 + a_5 s + a_6}$$

where

$$a_1 = L_{mo} \qquad a_2 = L_{mo}\left(\frac{2}{\tau_r} + \lambda_o^2 k_p\right)$$

$$a_3 = L_{mo}\left(\frac{1}{\tau_r^2} + \omega_{slo}^2 + \lambda_o^2 k_i + \lambda_o^2 \frac{k_p}{\tau_r} + \omega_{eo}^2\right)$$

$$a_4 = L_{mo}\left(\frac{2\omega_{eo}^2}{\tau_r} + \omega_{eo}^2 \lambda_o^2 k_p + \lambda_o^2 \frac{k_i}{\tau_r}\right)$$

$$a_5 = L_{mo}\left(\frac{\omega_{eo}^2}{\tau_r^2} + \omega_{eo}^2 \omega_{slo}^2 + \omega_{eo}^2 \lambda_o^2 k_i + \omega_{eo}^2 \lambda_o^2 \frac{k_p}{\tau_r}\right)$$

$$a_6 = \omega_{eo}^2 \lambda_o^2 \frac{k_i}{\tau_r}$$

$$b_1 = L_{ro} k_p \alpha_1$$

$$b_2 = L_{ro}\left(k_i \alpha_1 + k_p \omega_{eo} \alpha_2 + k_p \frac{2\alpha_1}{\tau_r}\right)$$

$$b_3 = L_{ro}\left(k_i \omega_{eo} \alpha_1 + 2\frac{k_i \alpha_2}{\tau_r} + 2\frac{k_p \omega_{eo} \alpha_2}{\tau_r} + \frac{k_p \alpha_2}{\tau_r^2} + k_p \omega_{slo}^2 \alpha_2\right)$$

$$b_4 = L_{ro}\left(2\frac{k_i \omega_{eo} \alpha_1}{\tau_r} + \frac{k_i \alpha_2}{\tau_r^2} + k_i \omega_{slo}^2 \alpha_2 + \frac{k_p \omega_{eo} \alpha_1}{\tau_r^2} + k_p \omega_{slo}^2 \omega_{eo} \alpha_1\right)$$

$$b_5 = L_{ro}\left(\frac{k_i \omega_{eo} \alpha_1}{\tau_r^2} + k_i \omega_{slo}^2 \omega_{eo} \alpha_1\right)$$

$$\lambda_o^2 \triangleq \lambda_{qro}^2 + \lambda_{dro}^2 \qquad \tau_r \triangleq \frac{L_{ro}}{R_{ro}} \qquad \omega_{slo} \triangleq \omega_{eo} - \omega_{ro}$$

$$\alpha_1 \triangleq \lambda_{qro} i_{qso} + \lambda_{dro} i_{dso}$$

$$\alpha_2 \triangleq \lambda_{qro} i_{dso} - \lambda_{dro} i_{qso}$$

8.2 Rotor resistance

$$\frac{\Delta\hat{\omega}_r}{\Delta R_r} = \frac{d_1 s^2 + d_2 s + d_3}{c_1 s^3 + c_2 s^2 + c_3 s + c_4}$$

where

$$c_1 = 1 \qquad c_2 = \frac{2}{\tau_r} + k_p\lambda_o^2$$

$$c_3 = \frac{1}{\tau_r^2} + \frac{k_p\lambda_o^2}{\tau_r} + k_i\lambda_o^2 + \omega_{slo}^2 \qquad c_4 = \frac{k_i\lambda_o^2}{\tau_r}$$

$$d_1 = k_p L_{mo}\alpha_2$$

$$d_2 = k_p\omega_{slo}(L_{mo}\alpha_1 - \lambda_o^2) + k_i L_{mo}\alpha_2 + \frac{k_p}{\tau_r}L_{mo}\alpha_2$$

$$d_3 = k_i\omega_{slo}(L_{mo}\alpha_1 - \lambda_o^2) + \frac{k_i}{\tau_r}L_{mo}\alpha_2$$

8.3 Leakage inductances

$$\frac{\Delta\hat{\omega}_r}{\Delta L_{ls}} = \frac{e_1 s^4 + e_2 s^3 + e_3 s^2 + e_4 s + e_5}{a_1 s^5 + a_2 s^4 + a_3 s^3 + a_4 s^2 + a_5 s + a_6}$$

$$\frac{\Delta\hat{\omega}_r}{\Delta L_{lr}} = \frac{f_1 s^4 + f_2 s^3 + f_3 s^2 + f_4 s + f_5}{a_1 s^5 + a_2 s^4 + a_3 s^3 + a_4 s^2 + a_5 s + a_6}$$

where

$$e_1 = -L_{ro}\omega_{eo}k_p\alpha_1$$

$$e_2 = L_{ro}\omega_{eo}\left(-k_i\alpha_1 + k_p\omega_{eo}\alpha_2 - k_p\frac{2\alpha_1}{\tau_r}\right)$$

$$e_3 = L_{ro}\omega_{eo}\left(k_i\omega_{eo}\alpha_2 - 2\frac{k_i\alpha_1}{\tau_r} + 2\frac{k_p\omega_{eo}\alpha_2}{\tau_r} - \frac{k_p\alpha_1}{\tau_r^2} - k_p\omega_{slo}^2\alpha_1\right)$$

$$e_4 = L_{ro}\omega_{eo}\left(2\frac{k_i\omega_{eo}\alpha_2}{\tau_r} - \frac{k_i\alpha_1}{\tau_r^2} - k_i\omega_{slo}^2\alpha_1 + \frac{k_p\omega_{eo}\alpha_2}{\tau_r^2} + k_p\omega_{slo}^2\omega_{eo}\alpha_2\right)$$

$$e_5 = L_{ro}\omega_{eo}\left(\frac{k_i\omega_{eo}\alpha_2}{\tau_r^2} + k_i\omega_{slo}^2\omega_{eo}\alpha_2\right)$$

$$f_1 = k_p\left(\omega_{slo}\lambda_o^2 L_{mo}/L_{ro} + \lambda_{dro}v_{qso} - \lambda_{qro}v_{dso}\right)$$

$$f_2 = k_i\omega_{slo}\lambda_o^2 L_{mo}/L_{ro} + k_i\lambda_{dro}v_{qso} - k_i\lambda_{qro}v_{dso} + k_p\frac{k_p\omega_{slo}\lambda_o^2 L_{mo}}{\tau_r L_{ro}} + k_p\beta_1$$

$$f_3 = k_p\omega_{slo}\omega_{eo}^2\lambda_o^2 L_{mo}/L_{ro} + \frac{k_i\omega_{slo}\lambda_o^2 L_{mo}}{\tau_r L_{ro}} + k_p\beta_2 + k_i\beta_1$$

$$f_4 = \frac{k_p\omega_{slo}\lambda_o^2\omega_{eo}^2 L_{mo}}{\tau_r L_{ro}} + k_p\left(\frac{1}{\tau_r^2} + \omega_{slo}^2\right)\left(\lambda_{dro}\omega_{eo}v_{dso} - \lambda_{qro}\omega_{eo}v_{qso}\right) + k_i\omega_{slo}\lambda_o^2\omega_{eo}^2 L_{mo} + k_i\beta_2$$

$$f_5 = k_i\left(\frac{1}{\tau_r^2} + \omega_{slo}^2\right)\left(\lambda_{dro}\omega_{eo}v_{dso} - \lambda_{qro}\omega_{eo}v_{qso}\right)$$

$$\beta_1 = \lambda_{dro}\omega_{eo}v_{dso} - \lambda_{qro}\omega_{eo}v_{qso} + \frac{2}{\tau_r}\lambda_{dro}v_{qso} - \frac{2}{\tau_r}\lambda_{qro}v_{dso}$$

$$\beta_2 = \frac{2}{\tau_r}\left(\lambda_{dro}\omega_{eo}v_{dso} - \lambda_{qro}\omega_{eo}v_{qso}\right) + \left(\frac{1}{\tau_r^2} + \omega_{slo}^2\right)\left(\lambda_{dro}v_{qso} - \lambda_{qro}v_{dso}\right)$$

8.4 Magnetising inductance

$$\frac{\Delta\hat{\omega}_r}{\Delta L_m} = \frac{L_{mo}}{L_{ro}}\frac{g_1 s^4 + g_2 s^3 + g_3 s^2 + g_4 s + g_5}{a_1 s^5 + a_2 s^4 + a_3 s^3 + a_4 s^2 + a_5 s + a_6}$$

where

$$g_1 = k_p(k_1 + k_8)$$

$$g_2 = k_p k_6 + k_i k_5 - k_p k_9 + k_8 k_{10}$$

$$g_3 = k_i k_6 + k_p k_5\omega_{eo}^2 - k_9 k_{10} + k_8 k_{11}$$

$$g_4 = k_p k_6\omega_{eo}^2 + k_i k_5\omega_{eo}^2 - k_9 k_{11} + k_7 k_8$$

$$g_5 = k_i k_6\omega_{eo}^2 - k_7 k_9$$

$$k_1 = \left(v_{qso} - R_{so}i_{qso} - \omega_{eo}L_{so}i_{dso} - \omega_{eo}L_{ro}i_{dso} + 2\omega_{eo}L_{mo}i_{dso} - \omega_{eo}\lambda_{dro}\right)/L_{mo}$$

$$k_2 = \left(v_{dso} - R_{so}i_{dso} + \omega_{eo}L_{so}i_{qso} + \omega_{eo}L_{ro}i_{qso} - 2\omega_{eo}L_{mo}i_{qso} + \omega_{eo}\lambda_{qro}\right)/L_{mo}$$

$$k_3 = \left(R_{ro}i_{qso} - \omega_{slo}\lambda_{dro}\right)/L_{mo}$$

$$k_4 = \left(R_{ro}i_{dso} + \omega_{slo}\lambda_{qro}\right)/L_{mo}$$

$$k_5 = \lambda_{qro}k_4 - \lambda_{dro}k_3$$

$$k_6 = \lambda_{qro}\omega_{slo}k_3 + \lambda_{qro}k_4/\tau_r - \lambda_{dro}k_3/\tau_r + \lambda_{dro}\omega_{slo}k_4$$

$$k_7 = k_i/\tau_r^2 + k_i\omega_{slo}^2$$

$$k_8 = \lambda_{dro}k_1 - \lambda_{qro}k_2$$

$$k_9 = \lambda_{qro}\omega_{eo}k_1 + \lambda_{dro}\omega_{eo}k_2$$

$$k_{10} = 2k_p/\tau_r + k_i$$

$$k_{11} = k_p/\tau_r^2 + 2k_i/\tau_r + k_p\omega_{slo}^2$$